Overburden Stress Arch Elevation Effect Induced by Roof Cutting and Destress Technique in Coal Mine Longwall Panel and Its Control Mechanism to Entry Surrounding Rock

Jinzhao Liu[1] · Dongyin Li[1,2] · Xiangjun Chen[2,3] · Shen Wang[1,2] · Haitao Wang[4] · Yongjia Xu[4]

Abstract

The safe and efficient driving of the roadway along the gob is becoming an increasing challenge due to the influence of the integrity and bearing capacity of the side coal and rock mass in the gob under the roof cutting mining mode. The mechanism of protection of the gob-side roadway is shown by modeling the influence of roof cutting and the application of a destress technique on the lateral coal and rock mass zones. The distribution characteristics of stress, displacement, and fracture in the overburden are analyzed by numerical simulation method under the three working conditions. The results indicate (1) construction of row holes and blasting can form artificial structure's fracture plane above the roadway, which can effectively cut the connection of overburden. The artificial structure's fracture plane decreases the peak value of the lateral coal body's support pressure. The peak point and the critical location of the stress reduction area are both transferred to the deep part at the same time, providing adequate space for the gob-side roadway. (2) The stress arch foot in the lateral rock mass rises to the rock layer at the bottom of the roof cutting plane after top cutting, as does the high-pressure area of deviator stress. The fracture plane prevents lateral coal and rock mass instability and limits the negative effects of roof deformation above the gob-side roadway. (3) The triangle slip fracture zone moves to over the roof cutting drilling zone due to the fracture plane, showing a high position compared to its original zone.

✉ Jinzhao Liu
  liujz0371@126.com

  Dongyin Li
  lidongyin@126.com

  Xiangjun Chen
  chenxj0517@126.com

  Shen Wang
  wangshen@hpu.edu.cn

  Haitao Wang
  w211701020038@126.com

  Yongjia Xu
  1486383115@qq.com

[1] School of Energy Science and Engineering, Henan Polytechnic University, Jiaozuo 454003, China

[2] State Collaborative Innovation Center of Coal Work Safety and Clean-Efficiency Utilization, Jiaozuo 454003, China

[3] College of Safety Science and Engineering, Henan Polytechnic University, Jiaozuo 454003, China

[4] Henan Pingbao Coal Industry Co., Ltd., Henan 461700, China

1 Introduction

The study of the stress field is one of the most basic and important works in analyzing the stability of surrounding rock and the deformation and failure characteristics of surrounding rock in mining activity. It is of vast significance to tunnel excavation, strata control, and disaster prevention. Domestic and foreign experts have made significant achievements in the theory of ground pressure control. Xu et al. [1] established the "masonry beam" structure model of the rocky layer on the field and proposed the key theory of rock formation control. Xu et al. [2] established the key layer-breaking block "masonry beam" structure model, enriching the theory of the structure of the overburdened rock. Feng et al. [3] proposed a "block beam-half arch" control structure. Zheng et al. [4] established the roof structure of "masonry beams" in the short-distance coal seam. Huang et al. [5] established the structural models of "short masonry beam" and "step rock beam" in shallow seam stope. Wang et al. (67) proposed the structure of a "short

cantilever beam-articulated rock beam" for the roof of a large mining height stop. He et al. [8] put forward the theory of top-cutting and pressure-releasing coal pillar–free mining based on the theory of "top-cutting short arm."

In the aspect of the mining stress field, abundant research results have been obtained. Han et al. [9] studied the supporting pressure distribution characteristics of fully mechanized top coal caving face in the deep and very thick coal seam. Ren et al. [10] studied the change characteristics of the advanced bearing pressure of the shallow seams. Wang et al. (6, 7) designed the monitoring device for coal seam-stress and microseismic and obtained the evolution law for lateral bearing pressure. Gao et al. [11] and Wang et al. [12] revealed the distribution law of the mining stress field under various conditions, which provides theoretical support for roadway support and roof control. Zhao et al. [13] expounded on the influence of the structure of fractured rock mass on the deformation of old gob. Kong et al. [14] described the concept of the dynamic evolution of the caving roof form of the "positive-inverted triangle" in the gob. Sun et al. [15] proposed a "hyperbola-like" model for the movement of overburden in thick unconsolidated strata, which combined the movement of overburden with surface subsidence. Shi et al. [16] proposed a conceptual model of a "W"-shaped fissure arch in the overburden of coal seam mining.

To sum up, the scholars mainly analyze the displacement of overburden, the mechanical model of caving structure, and the stress distribution characteristics of surrounding rock under the condition of the uncut roof. However, there is a lack of research on the stress distribution law of overburden in top-cut pressure relief mining utilizing stress cutting of the surrounding rock, deviator stress migration, and artificially induced overburden caving [17]. Therefore, this paper uses the method of theoretical analysis, numerical simulation, and engineering practice to study it, which provides a solid and reliable basis for the study of roof cutting and destress technology in the coal mine, disaster prevention, and scientific utilization.

2 Materials and Methods

### 2.1 Overview of Test Working Face

Pingdingshan mining area is located at the southern edge of North China block, and its geographical location is shown in Fig. 1. The average thickness of hex-15–17 coal seams in the mine is 5.30 m, and there is a layer of gangue with an average thickness of 0.4 m in the middle. The average depth below ground surface of hex-$_{15-17}$ coal seams is 740 m, and horizontal to vertical stress ratio is 1.12. The conveyor roadway of the 12110 working face is the test site for roof cutting and pressure relief, and the ventilating roadway of the next working face is the gob-side roadway. The inclined length of the working face where the fracture plane is located is 277 m, and the average minable strike length is 1533 m. The pseudo roof and direct roof of the conveyor roadway are mudstones (0.6–1.0 m thick) and sand mudstone inter bedding (3.2–5.1 m thick) respectively. The basic roof is fine and medium-grained sandstone, with a thickness of 23.6–45.5 m and an average thickness of 29.6 m. The hardness coefficient value is 6~11. The columnar shape is shown in Fig. 2(a).

The design basis of the roof cutting height is on the basis of the overburden structure of the working face exposed by the drilling, determine the occurrence layer of the overlying hard rock layer through the calculation of the key layer to ensure that the lower key layer is cut off and the upper key
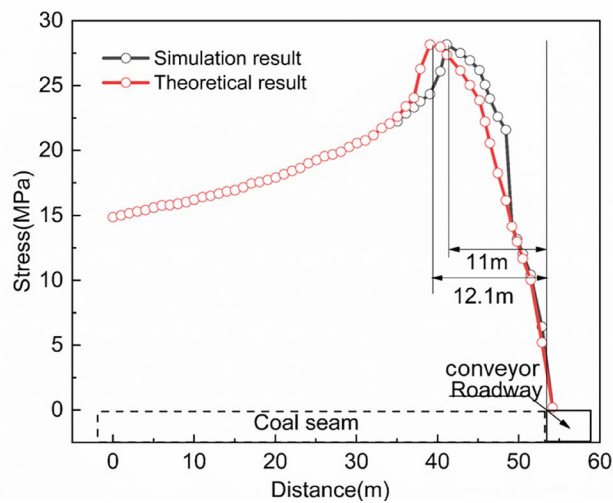
Fig. 1 Geographical location of the mining area
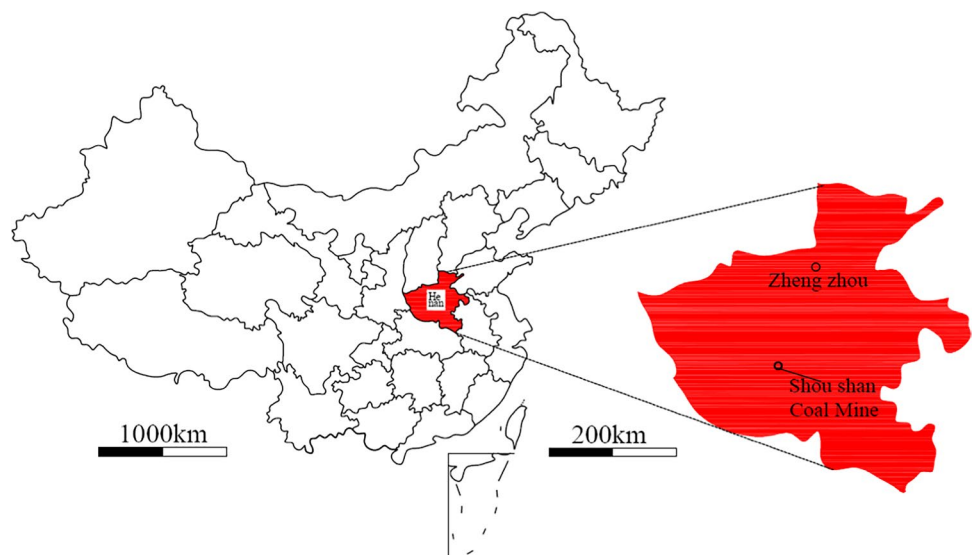
Fig. 2 Layout and model drawing of working face
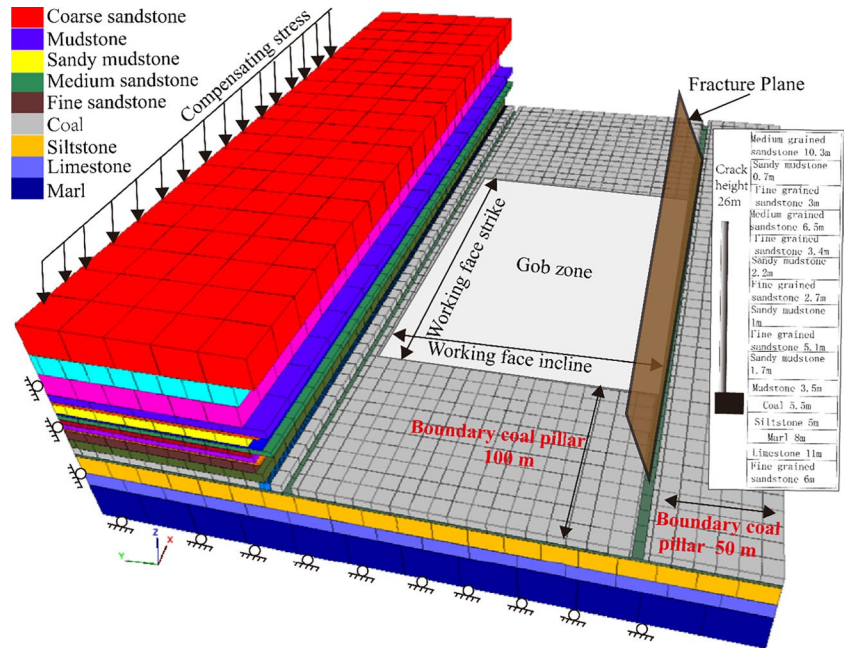
（a）Numerical model and legend

（b）Verification results

layer is retained. The roof cutting design height determined is the sand mudstone interbed 26 m above the machine roadway gateway of working face.

2.2 Establishment of the Numerical Model and Parameter Verification

2.2.1 Establishment of Numerical Model

A numerical calculation model is established according to the engineering geological conditions of the working face. The upper boundary applies a vertical downward boundary force,

the lower boundary is fixed in the vertical direction, and the horizontal direction of the boundary fixes the displacement by applying a force, as shown in Fig. 2(a). The width of the working face is 150 m and the thickness of the coal seam is 5.3 m. The model roof is composed of mudstone, alternating sandy mudstone, and fine and medium-grained sandstone from bottom to top. Mudstone is 3.5 m thick, and the cumulative thickness of sandy mudstone and fine-grained and medium-grained sandstone is 26.6 m. According to the exposure of geological drillings, the overburden is added to the model, with a cumulative thickness of 40.0 m. From top to bottom, the bottom plate is composed of argillaceous sandstone inter bedding with a

thickness of 5.0 m, marl with a thickness of 8.0 m, limestone with a thickness of 11.0 m, and fine-grained sandstone with a thickness of 6.0 m, in order to simplify the process of forming artificial structure's fracture plane after drilling and blasting, and ensure that the rock slides along the artificial structure's fracture plane. In the simulation, the construction process of the artificial structure's fracture plane adopts the method of deleting rock blocks, and the width of the deleted rock blocks is 0.3 m. This can simulate the discontinuous state of rock strata in the artificial structure's fracture plane.

2.2.2 Parameter Verification

To prove the reliability of model parameters, the width of elastic–plastic limit equilibrium in the coal pillar theory is introduced here. Based on the elastic–plastic limit equilibrium theory, the width of the elastic–plastic limit equilibrium zone is calculated, that is, Formula 1 [18, 19].

$$x_0 = \frac{\lambda M}{2 tan\varphi} \ln\left(\frac{k\gamma H + \frac{c}{tan\varphi}}{\frac{c}{tan\varphi} + \frac{P_x}{\lambda}}\right) \qquad (1)$$

where x_0 represents the width of the plastic zone, m; λ represents the horizontal stress coefficient, dimensionless; M is the coal seam thickness, m; c is the cohesion of coal seam, MPa; φ—friction angle of coal seam, degree; k is stress concentration factor, dimensionless; H is buried depth of coal seam, m; γ is average unit weight of overburden over the coal

seam, kN/m^3; P_x represents the roadway support resistance, MPa. According to the actual mining conditions of the working face, take $\lambda = 1.1$, $M = 5.3$ m, $c = 2.57$ MPa, $\varphi = 30.1°$, $k = 2.1$, $H = 740$ m, $\gamma = 0.025$ MN/m^3, $P_x = 0.5$ MPa, then $x_0 = 12.1$ m is calculated.

Before using the measured rock parameters for numerical calculation, it should be properly reduced and then verified through the width of the elastic–plastic limit equilibrium zone. The comparison between the results of the calculation example and the peak position of lateral bearing pressure ($x_0 = 11$ m) in the simulation results in Fig. 1(b) confirms the reliability of the model. The comparison of the results is shown in Fig. 1(b). The physical and mechanical parameters of the verified rock stratum are shown in Table 1, the joint surface contact adopts Mohr–Coulomb slip, and the mechanical parameters of the joint are shown in Table 2. This was achieved by conducting a series of unconfined compression tests on the numerical specimens (Fig. 3). The original rock mass parameters were first estimated based on the rock mass properties and then calibrated iteratively by numerical unconfined compression tests until the targeted elastic modulus and compressive strength listed in Tables 1 and 2 are attained. The optimal axial stress–axial strain curves of the numerical tests are displayed in Fig. 5. The calibrated Young's modulus value and the compressive strength value are listed in Table 3. It can be seen that the calibrated elastic modulus value and the compressive strength value were approximately equal to the targeted value. Therefore, the

Table 1 Physical and mechanical parameters of rock stratum

Rock stratum name	Elastic modulus/ GPa	Poisson's ratio	Tensile strength/ MPa	Cohesion/MPa	Internal friction angle/(°)	Density ρ/ (kg·m^{-3})
Medium sandstone	19.6	0.19	3.75	10.8	41	2331
Sandy mudstone	11.4	0.24	1.03	14.5	35	2361
Fine sandstone	14.27	0.23	4.22	18.6	38	2356
Coal	3.67	0.25	0.86	4.2	32	1380
Siltstone	20.14	0.23	2.51	11.8	33	2100
Marl	21.21	0.22	3.45	20.5	34	2167

Table 2 Physical and mechanical parameters of joints

Rock stratum name	Tangential stiffness/Pa	Normal stiffness/Pa	Tensile strength/ MPa	Cohesion/MPa	Internal friction angle/ (°)
Medium sandstone	19.5e11	19.5e11	1.25	17.8	28
Sandy mudstone	16.5e11	16.5e11	0.7	32	16
Fine sandstone	15.4e11	17e11	2.5	16	22
Coal	5.2e11	5e11	0.36	12	25
Siltstone	20.1e11	16e11	0.51	15	23
Marl	30e11	10e11	1.45	22.5	24
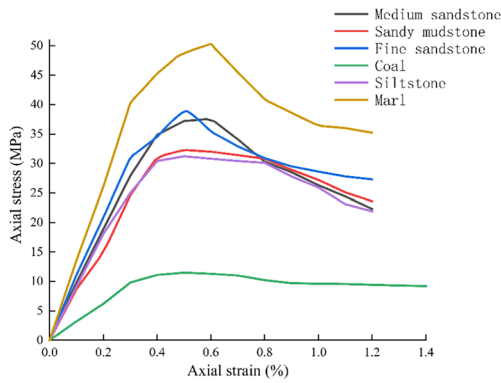
Fig. 3 Simulated unconfined compression tests and obtained optimal axial stress–axial strain curves

rock mass parameters listed in Table 1 and Table 2 could be applied to the mining model.

2.3 Numerical Simulation Analysis Method

According to the method of two-roadway non-cutting mining, the working faces of single roadway cutting mining and double roadway cutting mining are simulated to excavate, and the cloud diagram of vertical stress distribution is shown in Fig. 7. It should be noted that the coal seam horizon corresponds to the section Z-38~43.5 m in Fig. 7, and the position of the final drillings of the top-cutting drillings corresponds to the section Z-69.5~70 m in Fig. 7; the left and right boundaries of the working face correspond to the

Y-50 and Y-200 section in the slice in Fig. 7 respectively. The position of the working face and the bottom position of the top-cutting drillings are shown in Fig. 7(a). The conveyor roadway width corresponds to Y-50~55 section, and the ventilating roadway corresponds to Y-195~200 section.

For further analysis of data, six survey lines are arranged on the slice diagram in Fig. 7(a), in which the survey line Z-40 is located in the coal seam and parallel to the direction of the working face; survey lines Z-50, Z-69, and Z-100 are respectively located in the overburden and parallel to the direction of the working face; survey lines Y-45 and Y-205 are perpendicular to the working face.

3 Results and Discussion

3.1 Analysis of the Roof Broken State of the Mining Boundary

According to the theory of elastic thin plate with small deflection, the movement law of the roof is analyzed. The traditional mining method, single-side roof cutting and pressure relief mining, and two-roadway roof cutting and pressure relief mining have different boundary conditions for the first weighting and periodic weighting, and the corresponding mechanical model changes accordingly. Multiple hinged plate structures formed during the first weighting (Fig. 4) and periodic weighting (Fig. 5) of the main roof, and each hinged plate rotates and compresses the low hanging plate structure, resulting in large deformation of the surrounding

Table 3 Calibrated elastic modulus value and the compressive strength value in the model

Rock stratum name	Elastic Modulus (GPa)			Compressive Strength (MPa)		
	Target value	Calibrated value	Error (%)	Target value	Calibrated value	Error (%)
Medium sandstone	19.6	19.53	0.3	37.6	37.2	1.1
Sandy mudstone	11.4	11.35	0.4	32.3	32.0	0.9
Fine sandstone	14.27	14.21	0.4	38.8	39.2	1.0
Coal	3.67	3.62	1.3	11.5	11.8	2.6
Siltstone	20.14	20.08	0.2	31.2	31.5	0.9
Marl	21.21	30.15	0.2	50.3	50.9	1.2
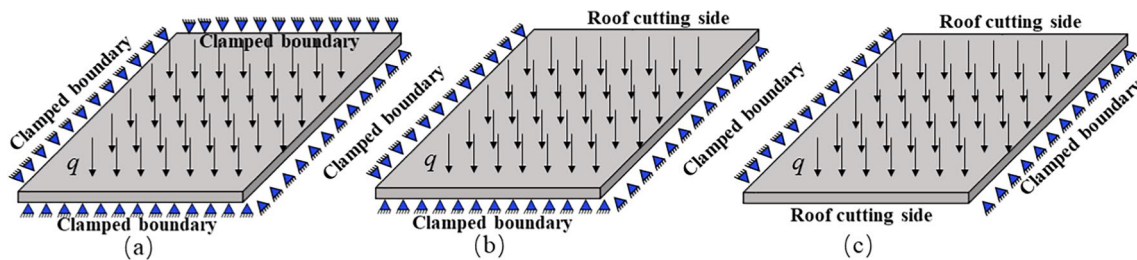
Fig. 4 Boundary condition for the first weighting; (a) not roof cutting, (b) single-side roof cutting, and (c) two-roadway roof cutting
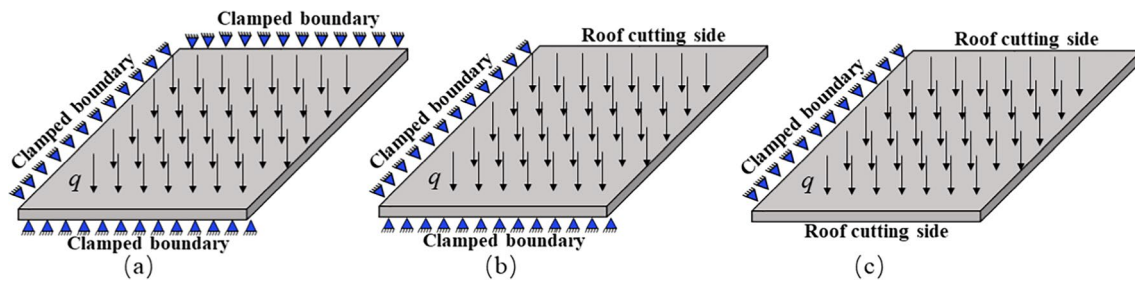
Fig. 5 Boundary condition for the periodic weighting; (**a**) not roof cutting, (**b**) single-side roof cutting, and (**c**) two-roadway roof cutting

rock of the roadway. When the roof is not cut, the roof forms a triangular hinge structure, which is equivalent to the fixed support boundary; when cutting the roof, there is no hinge plate at the roof cutting side, which is equivalent to the free boundary. The directional continuous artificial crack can effectively eliminate the triangular hinged plate structure of the roof, thus reducing the pressure of the coal pillar to the maximum extent, thus enhancing the control level of the surrounding rock of the roadway, weakening or even avoiding large deformation.

3.1.1 Mining Method of the Uncut Roof in Two Roadway

For the mining method of the uncut roof of roadway, the roof is broken by tensile stress to form rock blocks and then collapsed and piled up to fill the gob. From the perspective of the size of the reserved coal pillar, the roadway layout can be divided into large coal pillar mining methods and small coal pillar mining methods. The coal mining method with large coal pillars is based on the theory of "masonry beam." Retaining large coal pillars can arrange the mining roadway in the original rock stress area far from the gob of the previous working face, to avoid the destruction of the roadway under the action of the lateral bearing pressure. The mining method of retaining small coal pillars is based on the theory of "transfer rock beam." The theory believes that the lateral coal body will form the internal and external stress fields, and arrange the section of roadway in the low-stress area, the first weighting field (Fig. 4(a)), to maintain the stability of the roadway. From the view of the thin plate theory, the breaking state of its roof is the four sides of the basic roof are fixed constraints at the first weighting [20]. When periodic weighting (Fig. 5(a)), the basic roof is the free constraint on the side of the gob, and the other three sides are fixed constraints, that is, the three sides are fixed and one side is free.

3.1.2 Mining Method of Single Roadway Roof Cutting

Single roadway roof cutting mining means arranged blasting roof cutting drillings on the solid coal side of the mining

roadway (machine roadway) on one side of the working face, conducting advanced pre-splitting blasting on the roof of the working face to form a pre-splitting seam surface, cut off the connection between the roadway roof and the solid coal side roof, and make the roof slide down along the seam surface. Under the condition of this mining method, the peak pressure of the mined-out area is reduced and transferred to the deep, and the range of the stress reduction area is increased, which provides a safe stress environment for driving the gob-side roadway. The breaking state of the roof is analyzed from the perspective of thin plate theory: during first weighting (Fig. 4(b)), under the condition of cutting the roof on one side of the working face, the cutting side of the basic roof is simply supported constraint, while the other three sides are fixed constraint, that is, the three-sided fixed one side simply supported. During periodic weighting (Fig. 5(b)), it is assumed that the top-cutting side is simply supported, the gob side is free restraint, and the other two sides are fixed constraint, that is, the adjacent side is fixed, the side is simply supported, and the side is free.

3.1.3 Mining Method of Double Roadway Roof Cutting

Double roadway roof cutting and pressure relief mining means that arranged blasting roof cutting drillings in the two mining roadways in front of the working face, pre-splitting blasting is carried out on the roof of the working face and a pre-fracture plane is produced. Under the condition of two-roadway top-cutting mining, after the stress transfer path of the direct roof and the basic roof is blocked, the fracture position of the basic roof is transferred to the side of the mined-out area, the disturbance of the key block rotating subsidence to the roadway roof is weakened, and the layout of the roadway and the top-cutting line are shown in Fig. 6. Moreover, the breaking state of the first weighting and periodic weighting is changed from the original "O-X" shape to the approximate "rectangle" structure [20]. The breaking state of the roof is analyzed from the view of thin plate theory: during first weighting (Fig. 4(a)), the basic top is simply supported constraint on the cutting top side and fixed on the other two sides, that is, fixed to the side and simply
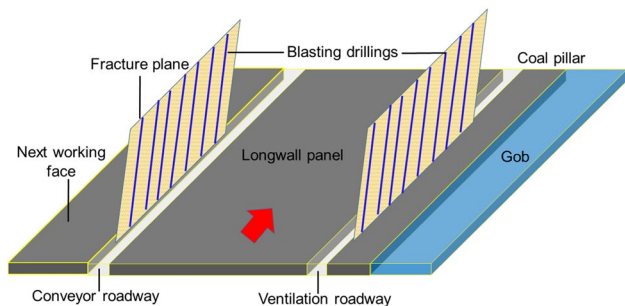
Fig. 6 Schematic diagram of double roadway cutting and pressure relief mining

supported to the side. During periodic pressure (Fig. 5(c)), the basic roof is simply supported constraint at the boundary of two cut-top sides, and the boundary of the gob side is a free constraint and the other side is a fixed constraint, that is, the opposite side is simply supported and the other side is fixed.

3.2 Analysis of the Characteristics of Coal and Rock Mass on the Side of the Working Face

It can be seen from Fig. 7(a): the stope space of the two-roadway non-cutting top mining method collapses to the gob with the collapse angle of 74–79° (shown in the red dotted line box and forms the blue pressure relief area in Fig. 7). At the same time, there is a stress concentration area in the lateral coal and rock mass, as shown in the rectangular black dotted line box in Fig. 7.

From Fig. 7(b) and (c) that the artificially constructed slit surface above the conveyor roadway and ventilating roadway makes the lateral stress concentration area in the coal seam

Fig. 7 Numerical simulation results of vertical stress distribution
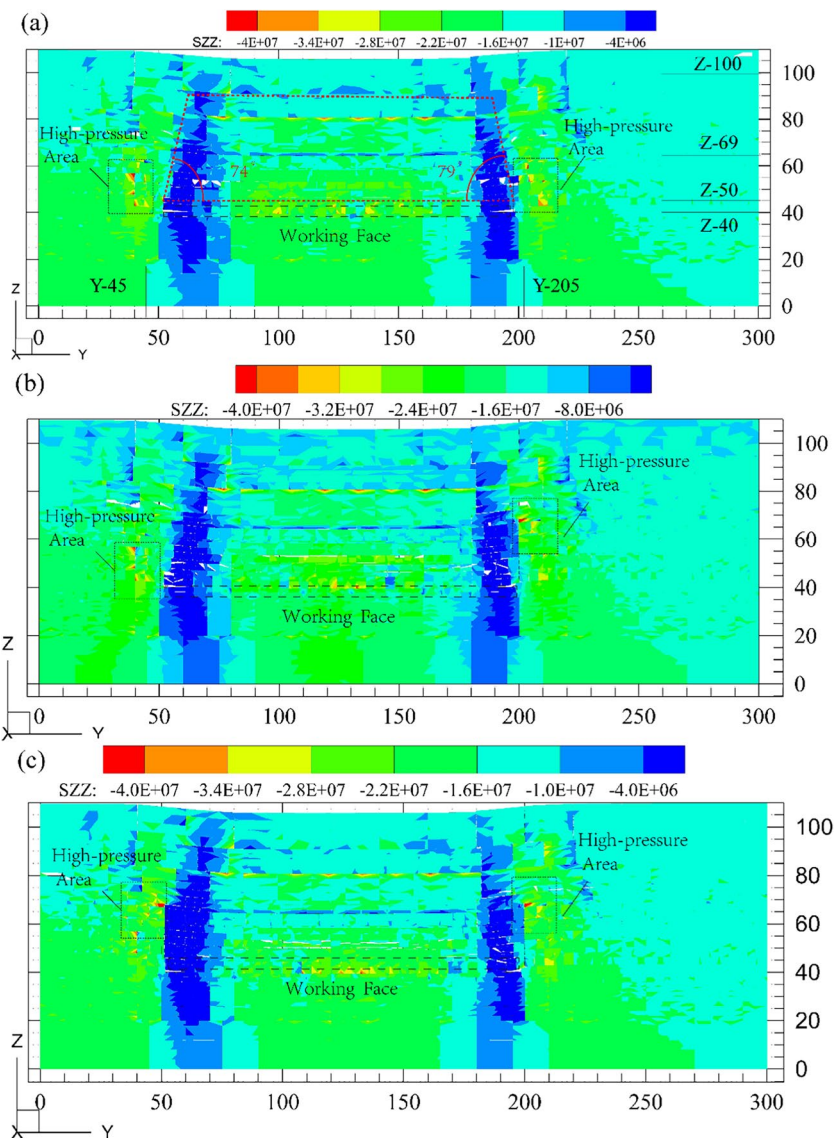
migrate to the rock stratum at the bottom of the top-cutting drillings, reducing the peak area of lateral stress in the coal seam. The existence of the cutting seam surface makes the pressure relief area of the roadway overburden develop along the seam line, and finally form a structural roof pressure relief area.

3.2.1 Influence of Roof Cutting on Vertical Stress of Coal Seam

The stress change curve can characterize the loading and unloading behavior after the mining stress of the coal seam is stable. Here, the vertical stress distribution data of coal and rock strata on the horizontal monitoring line of $Z = 43$ m (coal seam) in the model is extracted and analyzed.

It can be seen from Fig. 8: the peak area of lateral stress in the coal seam of the traditional mining method is 28 MPa, and the stress concentration factor can reach 1.87. After one-side roof cutting and pressure relief mining, the peak stress is reduced to 24 MPa, with a reduced range of 14.3%. After bilateral roof cutting and pressure relief mining, the peak stress on both sides is reduced to 24 MPa, and the stress concentration factor is reduced to 1.6. At the same time, the position of the stress peak point shifts to the deep part of the gob, and the width of the corresponding stress reduction area increases. This shows that blasting roof cutting can reduce the lateral stress concentration in the coal seam, improve the stability of coal and rock stratum, and provide space for stress reduction for the layout of the gob-side roadway.

With the advance of the working face, the stress of the upper overburden in the gob changes dynamically with the expansion of the caving area, and the stress change of the coal and rock strata on both sides of the gob presents a symmetrical bearing pressure distribution. Here, the stress data on the Z-69 measuring line near the final drillings position of the top-cutting drillings are extracted and summarized into a curve, as shown in Fig. 9. Comparing the stress on the Z-69 measuring line of the traditional mining method in Fig. 9 with the stress on the Z-69 measuring line of the unilateral roof cutting and pressure relief mining in Fig. 9,
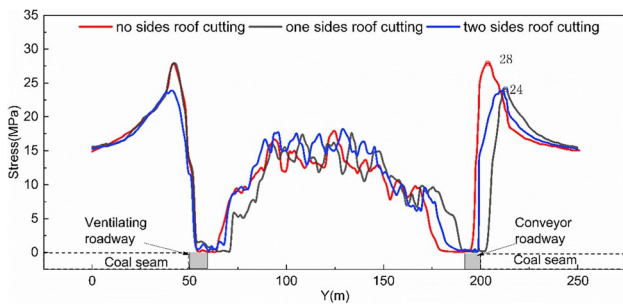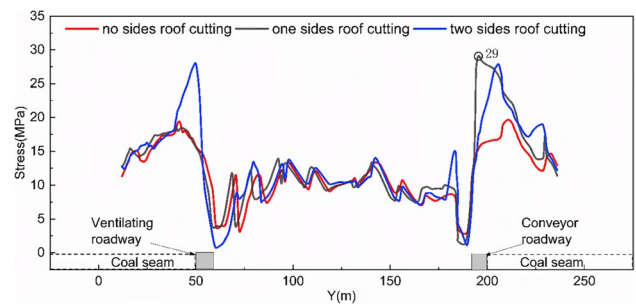

Fig. 9 Stress distribution curve in dip direction (Z-69 survey line horizon at the bottom of top-cutting drillings)

it can be seen that the roof cutting and pressure relief of the conveyor roadway (at the abscissa Y-200 m) caused the vertical stress in the rock stratum on this side to increase from 20 to 29 MPa, with an increase of 45%; from the changing trend of stress curve, the rock above the working face of the two mining methods also shows overburden pressure relief state after collapse and instability. Comparing the stress of one-side roof cutting and pressure relief mining with that of two side roof cutting and pressure relief mining in Fig. 9, the existence of two side roof cutting line blocks the stress transmission of the rock strata on both sides of the fracture plane, and presents a symmetrical supporting stress change curve in the rock strata at the end of the roof cutting drillings.

3.2.2 Elevation Effect of Pressure Arch Foot in the Lateral Rock Mass

According to the pressure arch theory, the excavation unloading area is within the boundary of the pressure arch, and the original rock stress area is outside the pressure arch boundary. Analysis from the mechanical model:
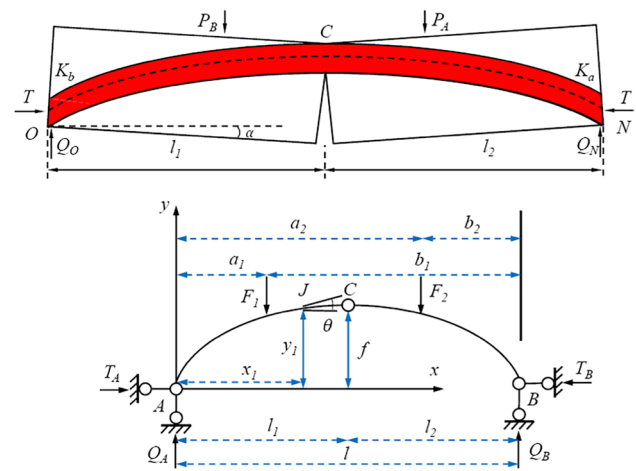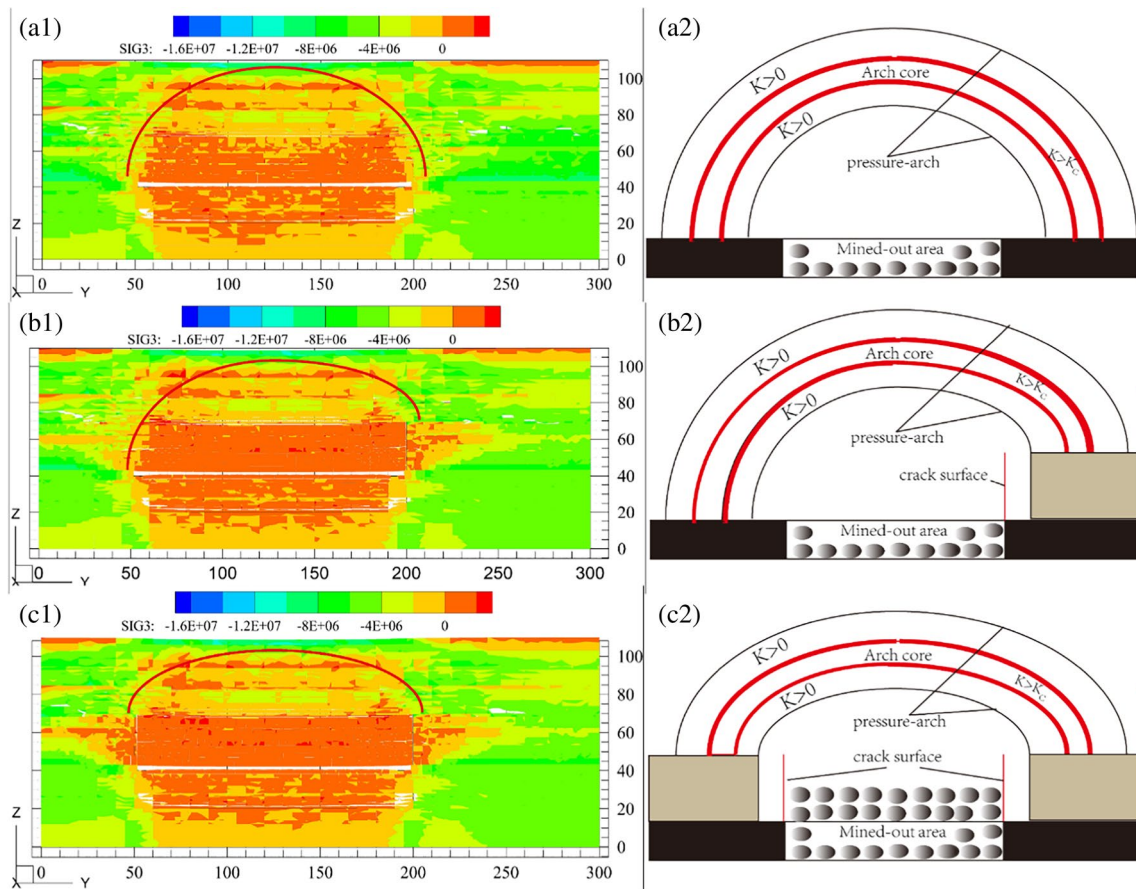

Fig. 8 Stress distribution curve in the dip direction

Fig. 10 Hinged arch structure of key blocks in fractured rock stratum

Fig. 11 Comparison between horizontal principal stress distribution under three conditions; (**a1, a2**) non-roof cutting working face, (**b1, b2**) conveyor roadway roof cutting working face, and (**c1, c2**) the top-cut working face of both the conveyor roadway and the ventilating roadway

the mining face continues to advance from the open cut drillings, and cracks will occur at both ends of the rocking beam and the middle of the rock beam span before the initial fracture. Under the condition of no sliding and instability, fracture block of rock beam to make the fault blocks squeeze each other. From Fig. 10, the fault block relies on the interaction of horizontal force t and vertical stress between contact surfaces to maintain static balance. When the roof of overburden reaches the critical state of limit span, the fault block of basic roof strata forms an asymmetric three hinge arch self-supporting structure [21].

According to the overall balance state of the three-hinged arch structure, the moment balance equations $\sum M_A = 0$ and $\sum M_B = 0$ at points A and B at the left and right arch feet can be obtained. By solving the moment balance equation, the vertical reaction forces Q_A and Q_B of the two supports can be obtained as Formulas (2) and (3):

$$Q_A = \frac{F_1 b_1 + F_2 b_2}{l} \tag{2}$$

$$Q_B = \frac{F_1 a_1 + F_2 a_2}{l} \tag{3}$$

In Formulas (2) and (3), F_1 and F_2 are the left half arch load and the right half arch load, kN/m; a_1, a_2, b_1, and b_2 are the force arms from loads F_1 and F_2 to left and right hinge points A and B, m; l in the span of three-hinged arch, m.

According to the equilibrium state of the left half arch, $\Sigma M_C = 0$ can be obtained. By solving the equilibrium equation, the horizontal reaction T_A of the left support can be obtained as Formula (4):

$$T_A = \frac{F_1 a_1 l_2 + F_2 a_2 l_1}{fl} \tag{4}$$

In Formula (4), F is the arch height at hinge point C, m; l_1 and is the horizontal distance from the mid-span hinge point C to the hinge points A and B on the left and right sides, M.

In Fig. 10, the limiting effect of horizontal thrust T_A and T_B at the arch foot on lateral displacement maintains the balance of three-hinged arch structures of fault block. When the fracture plane blocks the transmission path of horizontal

Fig. 12 Deviation stress change of monitoring line under different top-cutting conditions. Ventilating roadway survey line corresponding to (a1), (b1), and (c1) and conveyor roadway survey line corresponding to (a2), (b2), and (c2)
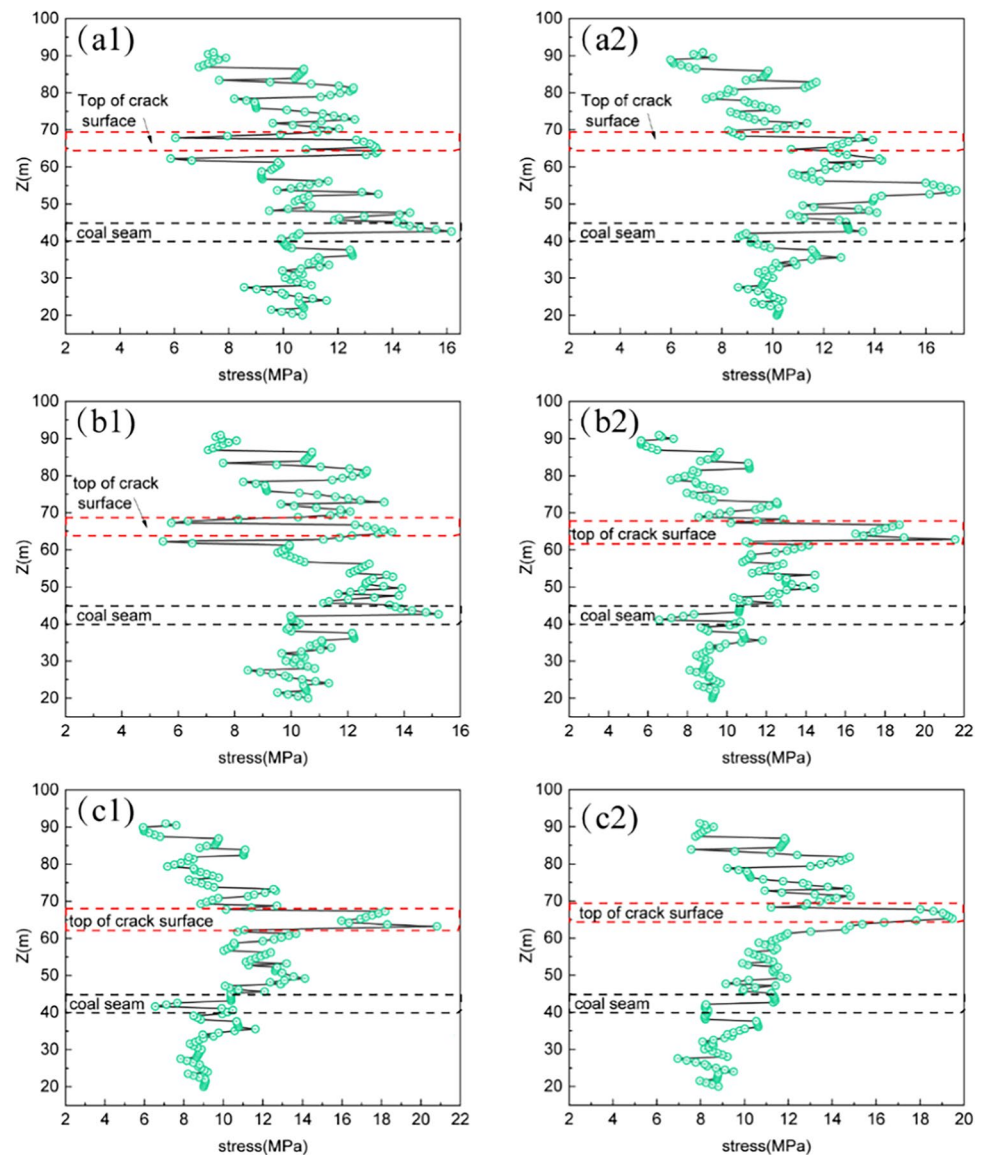
thrust, the extrusion force is no longer continuously transmitted. The state of the boundary of the compression zone in the fault block concentration starting and ending at the end of the contact surface on the left and right sides of the fault block changes. Without horizontal restraint compressive stress, the arching effect cannot exist. However, the existence of the fracture plane causes the effective transmission path of the horizontal force of the support on the cutting side to rise into the overburden on the upper part of the fracture plane. making the load to be transmitted to the arch foot on the other side along the high arch line; finally, a high-pressure arch is formed.

To prove the lifting phenomenon of the pressure arch foot, the cloud map slices of the principal stress distribution that did not reach the full mining stage in the early stage of mining were extracted, and the arch forming index K_C of the far-field pressure arch was used to describe the shape of the stress arch, where $k > K_C$ is the arch core area, and $K_C > k > 0$ is the secondary bearing area of pressure arch. From the morphological analysis, it can be seen that the main stress concentration area of the two-roadway non-roof cutting mining method takes the rock mass outside the working face as the arch foot and develops above the overburden, while the blasting roof cutting reduces the horizontal main stress of the coal and rock mass outside the roof cutting height range. The horizontal principal stress in the rock above the position of the final drillings of the top-cutting drillings increases, resulting in an area of high principal stress increase, which indicates that the arch foot area of the pressure arch jumps upward to the bottom layer of the top-cutting drillings, as shown in Fig. 11(b) and (c). To sum up, the analysis shows that the existence of
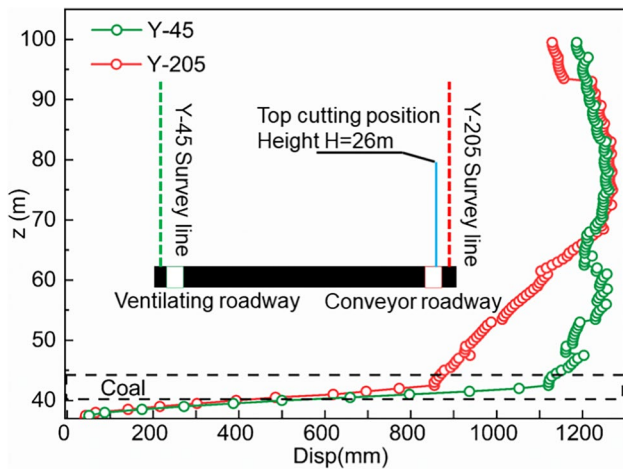
Fig. 13 Synthetic displacement of the vertical line

the top-cutting line causes the position of the arch foot of the stress arch to jump into the rock stratum of this layer with the increase of the height of the top-cutting plane, and the stress arch gradually changes from semi-circular (a) to flat (c).

3.2.3 Migration Law of Deviator Stress in Lateral Coal and Rock Mass

To confirm the uplifting phenomenon of the pressure arch described in the previous section, the eccentric stress from 20 m of the upper floor to 50 m of the roof of two vertical survey lines outside the mining roadway ($Y=45$ m and $Y=205$ m) is extracted. At the same time, the deviator stress theory in classical geotechnical plastic mechanics is introduced [22]. The theory holds that the stress of rock mass elements can be decomposed into spherical stress and deviator stress. Among them, spherical stress controls the volume deformation of the element, while deviator stress controls the shape deformation of the element. Therefore, deviator stress controls the plastic failure of rock mass elements, which is of great significance to the influence of plastic failure of the rock mass. It is known that the calculation Formula (5) of the maximum and minimum principal deviator stresses S_1 and S_3 is:

$$\begin{cases} S_1 = \sigma_1 - \sigma_m \\ S_3 = \sigma_3 - \sigma_m \\ \sigma_m = (\sigma_1 + \sigma_2 + \sigma_3)/3 \end{cases} \quad (5)$$

In Formula (5), S_1 and S_3 are the maximum and minimum principal deviator stresses, respectively; σ_1, σ_2, and σ_3 is the maximum, middle, and minimum principal stress of rock mass unit; σ_m is the average stress.

Figure 11(a1) and (a2) are the variation laws of deviation stress in the coal and rock mass on both sides of the working face in the model of a non-roof cutting working face. From Fig. 12(a), the peak values of the maximum deviator stress at the wide lane side (a1) and the conveyor roadway side (a2) of the uncut roof mining method can reach 16 and 17.5 MPa, respectively.

In the model of the conveyor roadway roof cutting working face, Fig. 11(b1) and (b2) show the variation law of deviation stress in the lateral coal and rock mass on both sides of the working face. As shown in Fig. 11(b), the peak deviation stress on the uncut top side of the ventilation roadway (b1) is still distributed in the coal seam, with the peak stress reduced to 15 MPa; and the peak deviation stress on the top of conveyor roadway (b2) is concentrated at the top of the fracture plane, with the peak deviation stress reduced to 22 MPa, with the coal seam deviation stress reduced to 11 MPa.

In the model of the top-cut working face of both the conveyor roadway and the ventilating roadway, Fig. 11(c1) and (c2) are the variation laws of the deviation stress in the coal and rock mass on both sides of the working face. As shown in Fig. 12(c), the eccentric stress on the top of the fracture plane at the side of ventilation roadway (c1) and conveyor roadway (c2) in the double roadway roof cutting and pressure relief mining method is concentrated, and the peak value can reach 20–21 MPa. At this time, the eccentric stress in the coal seams on both sides is reduced to 11 MPa. For the model shown in Fig. 12, the horizontal (vertical) joint division and block (joint) parameters are controlled invariants. Three different roof cutting conditions are variable. The results obtained have eliminated the influence of different material types, and the results are reliable. Through comprehensive analysis, it can be seen that roof cutting not only splits the mechanical connection of the "Arc triangle plate" at the working face ends but also transfers the high deviated stress in the coal seam to the hard rock, which maintains the integrity of coal seam and reduces the plastic deformation of coal roadway.

3.3 Deformation Characteristics of Mining Space and Engineering Examples

3.3.1 Lateral Rock Mass Extrusion and Overburden Fracture Development Characteristics

(1) Characteristics of lateral coal and rock extrusion
To better describe the influence of cutting top line on the displacement of lateral coal and rock mass after deformation, the Y direction displacement and Z direction displacement in the range of coal seam to roof 60 m are

Fig. 14 Dislocated fracture size and distribution histogram of overburden strata. (**a**) Traditional mining method, (**b**) one-side roof cutting and pressure-releasing mining method, and (**c**) the mining method of pressure relief by cutting the roof on both sides
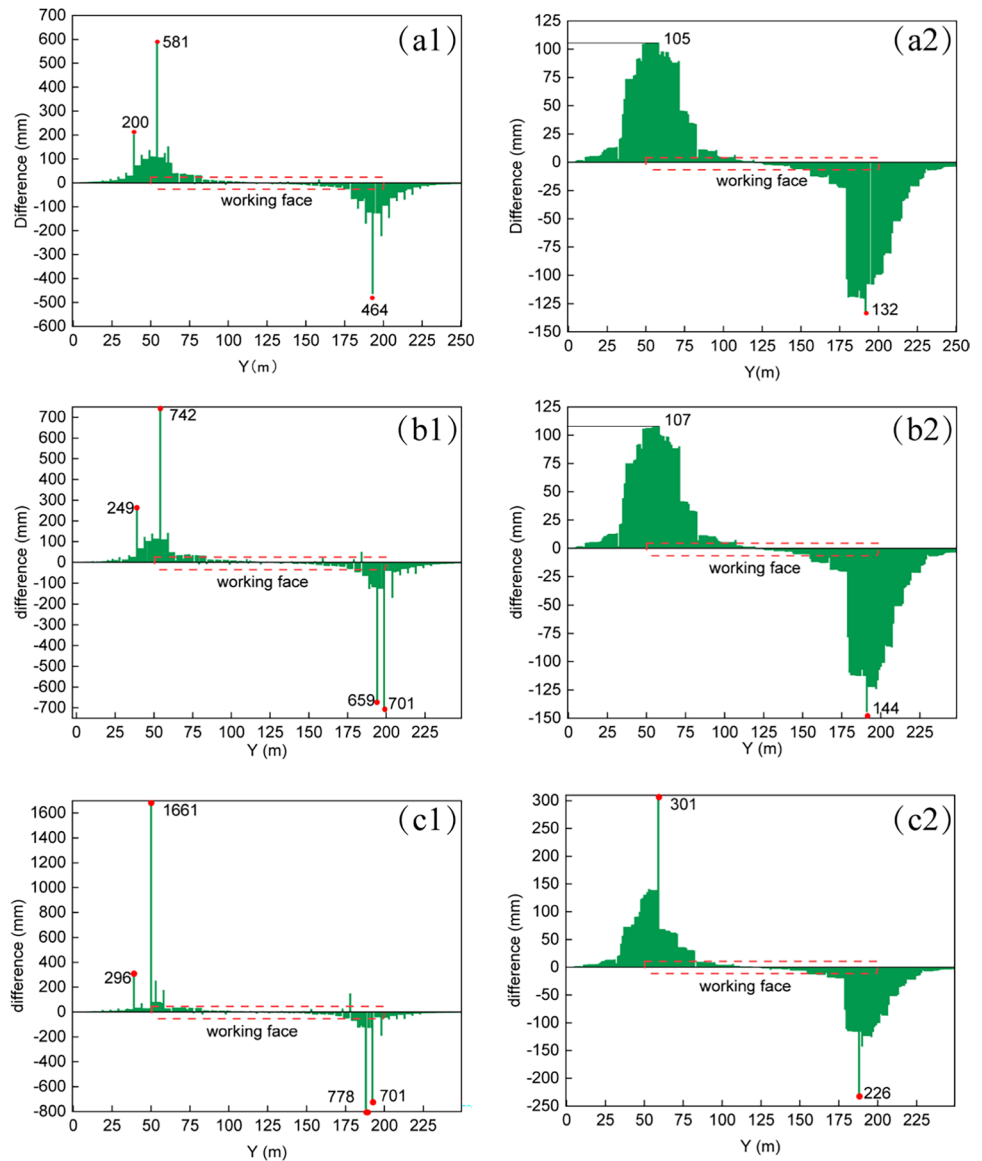

extracted from two vertical measuring lines ($Y = 45$ m and $Y = 205$ m), and the migration law of vertical strata is obtained by synthesizing the displacement vectors with the parallelogram rule as shown in Fig. 13.

As can be seen from Fig. 13, in the Z direction, the displacement of coal and rock mass on the top-cutting side of 40 (conveyor roadway roof level)–69 m is significantly less than that on the uncut topside, and the difference decreases in the range of 100–230 mm. In the Z direction, the displacement of coal and rock mass on the cutting top side to the gob within 69 (blasting drillings bottom level)–90 m is slightly greater than that on the uncut topside, and the difference develops steadily upward within 20 mm, In the Z direction, the displacement of the coal and rock mass on the cut topside to the

gob within 90–100 m is significantly less than that on the non-cut topside, and the difference develops in the range of 40–50 mm. This shows that the top-cutting surface cuts off the mechanical relation of overburden at, and limits the overall migration and expansion of the lateral coal and rock mass to the gob, and ensures the stability of the coal and rock mass at the roadway excavation position. Furthermore, the existence of a structural weak plane after roof cutting reduces the rotation and subsidence of overburden above the height of roof cutting and then controls the subsidence of overburden, which has a double effect.

(2) Distribution law of dislocated fracture

To get the displacement distribution characteristics of different strata, the displacement curves of $z = 50$ m (10 m above the coal seam) and $Z = 69$ m (rock strata near the
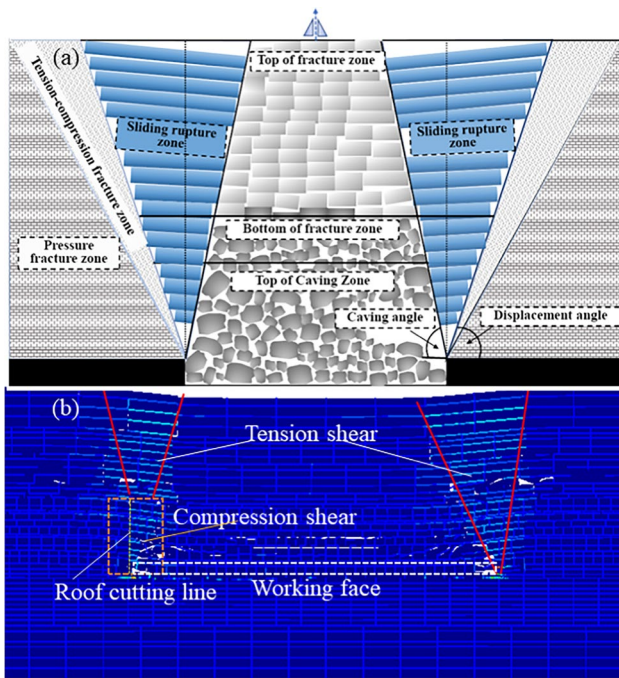
Fig. 15 The slip fracture zone

top-cut drillings bottom) were extracted. The displacement difference of adjacent data points is used to characterize the size and distribution of rock fracture. The figures are shown in Fig. 14.

From Fig. 14, the differential displacement values on the Z-50 line of 10 m overburden strata above the coal seam (Fig. 14(a1), (b1), and (c1)) show similar subsidence characteristics; the size of the crack through is generally larger (the maximum is in the range of 581–1661 mm). The displacement difference of the overburden strata in the 10 m layer above the coal seam (the size and distribution of the cracks running through) presents a normal distribution curve at the top and bottom of the seam without cutting the roof of the roadway. The maximum values of the size of the cracks running through are 581 mm and 464 mm respectively from Fig. 14(a1). In contrast to Fig. 14(a1) and (b1), it can be seen that the existence of the top-cutting line enlarges the transfixion of cracks in the overburdened strata at 10 m above the coal seam. From 464 to 701 mm in size, the same size of through fracture is formed at the adjacent position of the point. For example, there are two through fractures in the range of Y-175 to Y-200 m, the sizes of which are 659 mm and 778 mm respectively, see Fig. 14(b1) and (c1), respectively.

According to the difference of displacement on Z-69, the rocking beam in 26 m layer above the coal seam of two-roadway mining without cutting roof drillings is a continuous curved beam. The crack size and distribution

of the top and bottom end of the working face all show normal distribution curves, but the distribution curve of both sides of the top and the bottom end is not strictly symmetrical. However, a 144 mm staggered fracture drop appears in the overburden strata at 26 m above the top-cutting coal seam in a single roadway, which is 12 mm higher than the same position in Fig. 14(a2), as shown in Fig. 14(b2). However, the overburden strata at 26 m above the top-cut coal seam in the top-cut mining with two roadways have obvious staggered fracture drops of 301 mm and 226 mm on both sides of the top-cut coal seam. The through the size of the crack after the top cut of the side of the ventilation roadway is enlarged by 2.87 times, and the through the size of the crack after the top cut of the side of the conveyor roadway is enlarged by 1.71 times. The results show that the fracture plane increases the size of the through fracture and the size of the air–water outlet.

3.3.2 Characteristics of Slip Zone of Overburden Strata on the Working Face End

The lower cantilever beam–upper masonry beam structure (low key cantilever beam, high key masonry beam) is formed in the overburdened strata at the end of the working face before the gob is stable [23]. After the mined-out area is stable, the cantilever beam breaks and moves to the mined-out area, forming the triangle slip area. The caving zone, triangular slip rupture zone, tension fracture zone, and fracture zone are formed by the boundary of caving angle, displacement angle, boundary angle, and the peak value of lateral support pressure, as shown in Fig. 15(a).

To characterize the transformation effect of the surface of the blasting crack on the shear zone of the overburden strata, the model slices of the central strike of the stope are extracted. The aim is to analyze the variation of the regional distribution characteristics of the overburden strata in tension and shear (compression and shear), as shown in Fig. 15. From the analysis of Fig. 15(b), it can be seen that the overburden strata break and bend down toward the gob after the mining of the coal seam without top cutting; the upper and lower ends of the cantilever beam are broken to form a sliding fracture zone with the tip as the apex, the angle of collapse and the boundary angle as the two rays. When the rock movement is stable, a tension-shear fracture zone developed into a fracture zone, or a curved subsidence zone is formed, as shown on the right side of the working face in Fig. 15. The existence of the roof-fracture plane on the left side of the working face makes the roof cutting and falling overburden fill the space of the gob end-side in the way of a continuous

Fig. 16 Field photographs and comparison of surrounding rock deformation
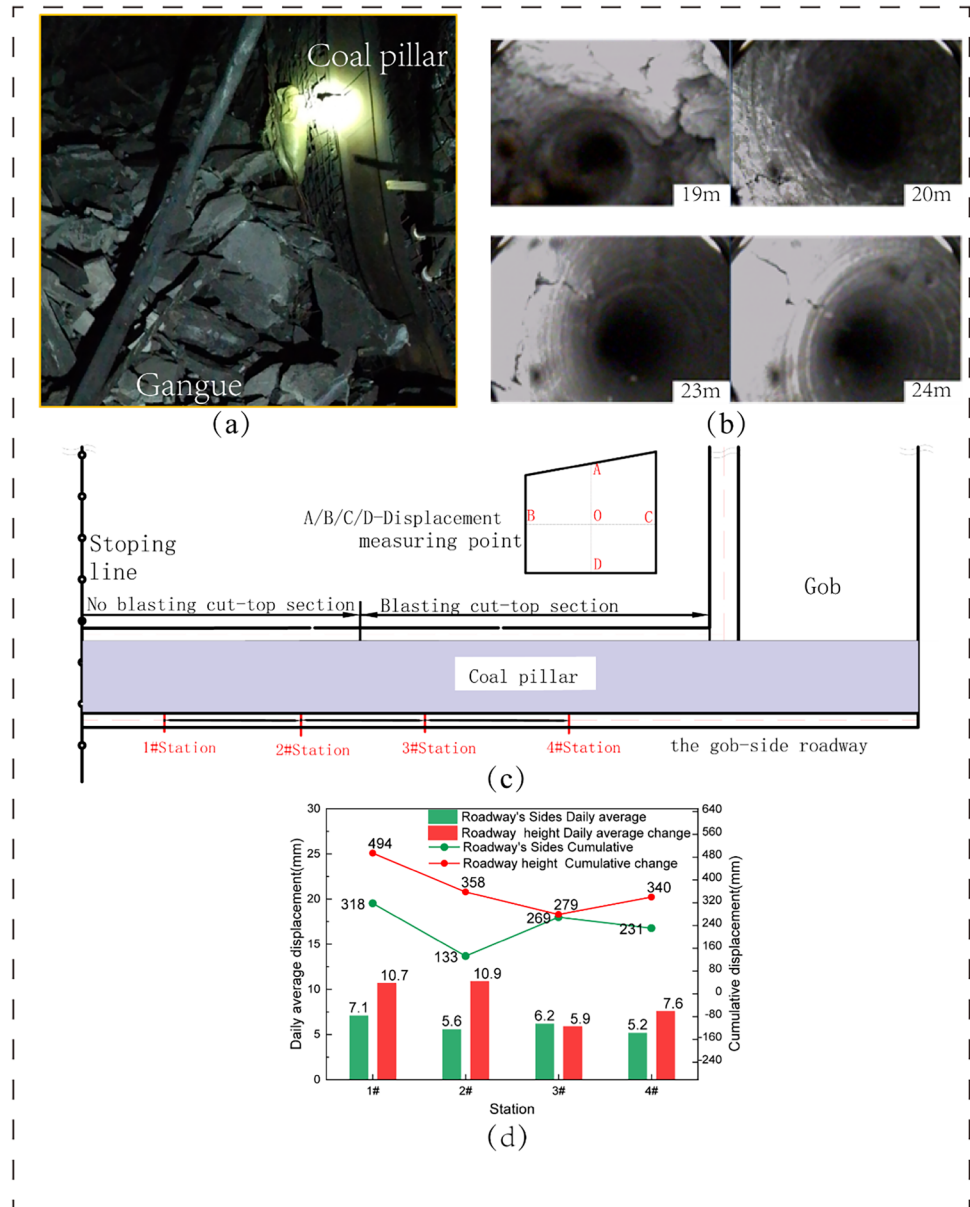
bending beam. A compression-shear zone (Fig. 15(b), rectangular box) is produced on one side under horizontal compressive stress, while a top-fracture plane causes no shear zone to develop in the lateral strata. On the other hand, the overburdened rock above the top of the top-fracture plane reforms a triangle-shaped slip fracture zone on the top of the top-fracture plane, and the triangle-shaped slip zone pattern developed from the base point to the surface and developed into a high-level position.

3.3.3 Engineering Demonstration

The site of the blasting cut-off test is chosen in the conveyor roadway of the working face. After the blasting cut-off, the conveyor roadway and the gob are filled by the gangue in time. The

field picture of the rear part of the bracket is shown in Fig. 16(a). The result of drillings after blasting is shown in Fig. 16(b). It can be seen that the fractures along the length of the drillings are developed after blasting. When the last working face is finished, the next working face will be excavated along with the gob and a survey station will be set up in the roadway. The position of the survey station is shown in Fig. 16(c). The 1–2 # station is in the non-blasting top-cutting section, and the 3–4 # station is in the blasting top-cutting section. From Fig. 16(d), it can be seen that the cumulative approaches of top and bottom plates in the non-pressure relief section are 494 mm and 358 mm respectively, with a mean of 426 mm, and 279 mm and 340 mm respectively, with a mean of 309.5 mm. The accumulative deformations of the two sides in the non-pressure relief section were 318 mm and 133 mm, respectively, with an average value of 225.5 mm.

The accumulative deformations of the two sides in the pressure relief section were 269 mm and 231 mm, with an average value of 250 mm. To sum up, although the deformation of the two sides of the roadway increased slightly after the blasting cut, the displacement of the roof and floor decreased by 27.3% compared with that of the non-pressure relief roadway.

4 Conclusions

(1) Numerical simulation confirms the existence of a stress arch effect in overlaying strata after coal seam mining. At the same time, the existence of the fracture plane causes the pressure arch foot to be lifted into the lateral rock mass at the bottom of the cut-top blasting drillings, and the stress arch is changed from a semicircle to a flat, as shown by comparing the horizontal stress distribution law under three conditions.

(2) The fracture plane reduces the peak stress in the coal seam by 14.3% and reduces the stress concentration coefficient from 1.87 to 1.6. The fracture plane causes the high deviating stress region in the coal seam to migrate to the hard roof above the fracture plane, reducing the deviating stress. The deformation and fracture development of the coal seam are terminated using roof cutting technology.

(3) The extrusion displacement of lateral coal and rock mass to the gob is greatly reduced due to the fracture plane, according to an investigation of the characteristics of the sliding zone and lateral rock mass extrusion at the end of the working face. The fracture plane causes a high-level slip fracture zone to emerge in the overloaded layers, increasing the stability of the gob-side roadway by ensuring the integrity and stress transfer of lateral coal and rock mass.

Data Availability The datasets during the current study are available from the corresponding author on reasonable request.

Declarations

Conflict of Interest The authors declare no competing interests.

References

1. Qu Q, Xu J, Wu R, Qin W, Hu G (2015) Three-zone characterisation of coupled strata and gas behaviour in multi-seam mining. Int J Rock Mech Min Sci. https://doi.org/10.1016/j.ijrmms.2015.04.018

2. Zhu L, Xu J, Ju J, Zhu W, Xu J (2018) The effects of the rotational speed of voussoir beam structures formed by key strata on the ground pressure of stopes. Int J Rock Mech Min Sci 108:67–79. https://doi.org/10.1016/j.ijrmms.2018.04.041

3. Feng G, Wang X, Kang L (2008) Analysis of the mechanism of the face-contacted blocks structure in overlying strata above the longwall face. J China Coal Soc 33(1):33–37. https://doi.org/10.1016/S1872-5791(08)60057-3

4. Zheng S, Lou Y, Kong D, Wu G, Liu Y (2019) The roof breaking characteristics and overlying strata migration law in close seams group under repeated mining. Geotech Geol Eng, 1–12. https://doi.org/10.1007/s10706-019-00879-0

5. Huang Q, Zhou J, Cao J (2020) Key stratum structure and support working resistance of longwall face with large mining height in the shallow coal seams, China. Adv Civil Eng 2020(3):1–14. https://doi.org/10.1155/2020/8834403

6. Wang S, Mao D, Pan J (2015) Measure mention the whole process of abutment pressure evolution and microseismic activities at the lateral strata of gob. J China Coal Soc 40(12):2772–2779. https://doi.org/10.13225/j.cnki.jccs.2015.0080

7. Wang W, Cheng YP, Wang HF, Liu HY, Wang L, Li W, Jiang JY (2015) Fracture failure analysis of hard–thick sandstone roof and its controlling effect on gas emission in underground ultra-thick coal extraction. Eng Fail Anal 54:150–162. https://doi.org/10.1016/j.engfailanal.2015.04.016

8. Wang Y, Gao Y, Wang E, He M, Yang J et al (2018) Roof deformation characteristics and preventive techniques using a novel non-pillar mining method of gob-side entry retaining by roof cutting. Energies 11:627. https://doi.org/10.3390/en11030627

9. Han H, Xu J, Wang X, Xie J, Xing Y (2019) Method to calculate working surface abutment pressure based on key strata theory. Adv Civil Eng 2019(6):1–20. https://doi.org/10.1155/2019/7678327

10. Ren Y, Ning Y (2014) Changing feature of advancing abutment pressure in shallow longwall working face. J China Coal Soc 39(S1):38–42. https://doi.org/10.13225/j.cnki.jccs.2012.1280

11. Gao M, Jin W, Dai Z, Xie J (2013) Relevance between abutment pressure and fractal dimension of crack network induced by mining. Int J Min Sci Technol 23(6):925–930. https://doi.org/10.1016/j.ijmst.2013.11.008

12. Wang H, Jiang Y, Deng B, Zhan S (2014) Study of the stress state of coal pillar in failure zone of coal seam under dynamic pressure of mining. Chin J Rock Mech Eng 33(10):2056–2063. https://doi.org/10.13722/j.cnki.jrme.2014.10.012

13. Zhao X, Zhao J, Cai J, Hefny A (2008) Udec modelling on wave propagation across fractured rock masses. Comput Geotech 35(1):97–104. https://doi.org/10.1016/j.compgeo.2007.01.001

14. Kong D, Li Q, Wu G, Song G (2021) Characteristics and control technology of face-end roof leaks subjected to repeated mining in close-distance coal seams. Bull Eng Geol Environ 80(11):8363–8383. https://doi.org/10.1007/s10064-021-02438-5

15. Sun Y, Zuo J, Karakus M, Wang J (2019) Investigation of movement and damage of integral overburden during shallow coal seam mining. Int J Rock Mech Min Sci 117:63–75. https://doi.org/10.1016/j.ijrmms.2019.03.019

16. Shi L, Xu D, Wang Y, Qiu M, Hao J (2019) A novel conceptual model of fracture evolution patterns in the overlying strata during horizontal coal seam mining. Arab J Geosci 12(10):326. https://doi.org/10.1007/s12517-019-4486-x

17. Zhao M, Zhu L, Huang Q, Xu K, Wu Y, Gu W (2022) Research on roof fracture characteristics of gob-side entry retaining with roof cutting and non-pillar mining in thick coal seam, China. Geotech Geol Eng 40(3):1429–1448. https://doi.org/10.21203/rs.3.rs-484570/v1

18. Wang R, Bai JB, Yan S, Chang ZG, Wang XY (2020) An innovative approach to theoretical analysis of partitioned width & stability of strip pillar in strip mining. Int J Rock Mech Min Sci 129:104301. https://doi.org/10.1016/j.ijrmms.2020.104301

19. Zhu J, Ma Z (2011) Calculation and application on elastic-plastic coal pillar width of the stope. Metal Mine 26:1116–1124. https://doi.org/10.1016/j.proeng.2011.11.2282

20. Guo S, Tai Y, Wang Z, Shi B, Yang K (2021) Fracture characteristics of basic roof and mechanism of strata behavior in a pillarless working face. J Geophys Eng 18(6):875–889. https://doi.org/10.1093/jge/gxab059

21. Wang S, Wu X, Zhao Y, Hagan P, Cao C (2019) Evolution characteristics of composite pressure-arch in thin bedrock of overlying strata during shallow coal mining. Int J Appl Mech. https://doi.org/10.1142/S1758825119500303

22. Shan R, Li Z, Wang C et al (2021) Study on the distribution characteristics of stress deviator in the surrounding rock when mining closely spaced coal seams. Environ Earth Sci 80:602. https://doi.org/10.1007/s12665-021-09891-1

23. Wang Y (2017) Evolution mechanism of end structure and abutment pressure on fully-mechanized top coal caving face in extra-thick coal seam. J China Coal Soc 42(S1):30–35. https://doi.org/10.13225/j.cnki.jccs.2016.1086